Astron. Astrophys. 323, 986–998 (1997)

ASTRONOMY AND ASTROPHYSICS

Dynamics of comets in the outer planetary region

II. Enhanced planetary masses and orbital evolutionary paths⋆

G.B. Valsecchi[1,2] **and A. Manara**[3]

[1] Observatoire de la Côte d'Azur, B.P. 229, F-06304 Nice, France
[2] I.A.S. – Planetologia, viale dell'Università 11, I-00185 Roma, Italy
[3] Osservatorio Astronomico di Brera, via Brera 28, I-20121 Milano, Italy

Received 24 May 1996 / Accepted 5 July 1996

Abstract. We study the effect of increasing the masses of the outer planets to speed up the numerical integration of orbital evolutions of fictitious comets subject to planetary close encounters. We use Öpik's theory to model encounters on crossing orbits, and find that the distribution of energy perturbations, and especially of its tails, is changed significantly depending on the range of initial conditions considered and on the enhancement factor used for the planetary masses. We then analyze nearly tangent, low-velocity encounters making use of a simple argument based on the opening of Hill's surfaces of zero velocity, again finding that the energy perturbation distribution depends on the mass enhancement factor. To check these results we compare the outcomes of integrations done with masses enhanced by the factors 10 and 40 to those of integrations done with the real masses, coming once more to the same conclusion; we put these findings in perspective, discussing the more general issue of the dynamical paths followed by potential short-period comets in the region of the outer planets. Results concerning the orbital evolution of comets obtained by integrations performed with enhanced masses should be considered with caution.

Key words: comets: general – celestial mechanics

1. Introduction

The source regions so far envisaged for the two main components of the population of short-period comets, i.e. the Halley-type (HT) ones, with orbital periods P such that $20 < P < 200$ yr, and with inclinations of any value, and those belonging to the Jupiter-family (JF), with $P < 20$ yr, and with small inclinations, are the spherically symmetrical, centrally condensed inner core of the Oort cloud (Bailey and Stagg 1990), and the so-called Edgeworth-Kuiper belt, a disc-like reservoir immediately outside the orbit of Neptune (Fernández 1980; Duncan et al. 1988; Quinn et al. 1990). In order to discriminate between them it is crucial to understand how multi-stage capture, i.e. the process by which potential short-period comets are passed from the dynamical control of one planet to that of the next inner one, takes place; these transfers are essentially due to close encounters with the controlling planet, unless the approaches are prevented by resonances or by peculiar orbital arrangements.

While to derive the HT comets from an isotropic source like the inner Oort cloud does not appear to pose major problems, it seems not as easy to get from that source the low inclination JF comets; the mechanism advocated for this task is the rapidly diminishing capture rate for larger inclinations (Bailey and Stagg 1990). However, this is contradicted by Quinn et al. (1990), who computed the orbital evolutions of many thousand comets perturbed by the four giant planets, starting from orbits having semimajor axis a = 50 AU, perihelion distance q uniformly distributed between 20 and 30 AU, and cosine of inclination i uniformly distributed either between 0.95 and 1, to simulate a disc-like source, or between 0 and 1, to simulate a prograde isotropic source (orbits with $-1 < \cos i < 0$ were excluded for computational efficiency), and ending the integrations when orbits typical of the short-period comets were reached. Starting from the flattened source led to much better agreement with the observed population of short-period comets than starting from the isotropic one, since in this last case too many HT comets were produced and the distribution of inclinations of JF comets was not reproduced well enough (note that the very important issue of the observational completeness of the two periodic comets populations was essentially not touched in that work).

To reduce the computer time required by their very long integrations, Quinn et al. (1990) used a solar system composed of only the four outer giant planets on circular orbits, multiplying the planetary masses by a factor μ = 10; according to them, this would speed up significantly the orbital evolution, that they considered to be modelizable like a diffusion process. Quinn

Send offprint requests to: G.B. Valsecchi

⋆ Appendix A and B are only available in electronic form at http://cdsweb.u-strasbg.fr/abstract/htlm

et al. discussed various ways in which the orbital evolution in their model may have been altered by the mass enhancement compared to the case with the real masses, concluding that the main features of the problem should not have been affected, and supporting this conclusion also with the similarity of the results obtained using $\mu = 40$.

Bailey and Stagg (1990) questioned the possibility of treating the multi-stage capture of comets as a diffusion process, since many comets undergo very close encounters with the planets that drastically change their orbital elements, and that are better modelled as a stochastic process. In this case, the end states of the evolution are essentially determined by the asymmetries of the tails of the distribution of energy perturbations, discovered by Everhart (1969; Oikawa and Everhart 1979), and changing the masses of the planets can alter, as Bailey and Stagg (1990) argue, these distributions.

In this paper we show that in fact the distribution of energy perturbations at close planetary encounters, a key feature of any model attempting to reconstruct the orbital evolution of comets, is significantly altered if the masses of the perturbing planets are increased beyond a certain value. We do this in several ways: using Öpik's theory of close encounters, in the case of initially crossing orbits (Sect. 2), by comparing the perturbation distributions obtained from numerical integrations using enhanced masses to those obtained with the unenhanced masses (Sect. 3), and basing on results coming from studies of the evolution of some peculiar short-period comets, interpreted in the framework of the restricted circular three-body problem, in the case of non-crossing orbits (Sect. 4). Finally, in Sect. 5 these results are discussed in the context of the multi-stage capture of short-period comets, and in Sect. 6 the conclusions are given.

Let us remark here that Öpik's theory of close encounters has been used in this paper not only, as is customarily done, as a fast tool to compute close encounter outcomes, but above all as a geometric tool to explore the qualitative features of close encounter dynamics. With the increasing performances of modern computers, that make the computation of a large number of close encounters a less and less prohibitive task than it used to be, it seems to us possible that the importance of Öpik's theory as a computational tool will decrease compared to its importance for understanding close encounters outcomes.

2. Encounters on crossing orbits

We describe here the basic features of Öpik's treatment of close encounters on crossing orbits, following Carusi et al. (1990) and Valsecchi (1992a); a complete description of the theory can be found in Öpik (1976).

We start by assuming that the planet in question moves on a circular orbit of radius $a_p = 1$, and take the plane of its motion as reference plane; the massless particle moves on an orbit, with orbital elements a, e, i, ω and Ω, that crosses that of the planet in one of the nodes. The direction from the Sun to the ascending node of the particle's orbit is the reference direction, so that $\Omega = 0$, and both G, the constant of gravity, and M, the mass of the Sun, are set equal to 1; in these units the circular heliocentric velocity at $a = 1$ is $v_{circ} = 1$.

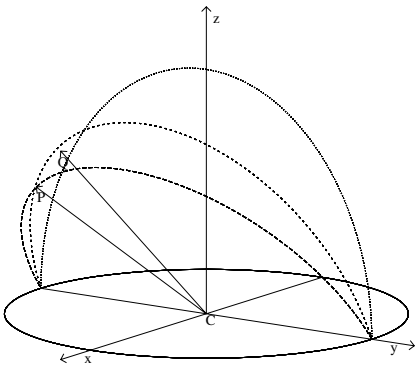

Fig. 1. The geometry of velocity deflection in the rotating frame centred on the planet; for the definitions of the various vectors and angles, see the text.

In a frame centred on the planet, with the z-axis perpendicular to the orbital plane of the planet, the y-axis in the direction of the planet's velocity and the x-axis pointing in the direction opposite to that of the Sun (see Fig. 1), the *unperturbed* encounter velocity $\boldsymbol{U}$ of the particle, i.e. the velocity it would have when encountering the planet if the acceleration due to the mass of the latter were discarded, has components:

$$U_x = U \sin\theta \sin\phi \tag{1}$$

$$U_y = U \cos\theta \tag{2}$$

$$U_z = U \sin\theta \cos\phi \tag{3}$$

where θ is the angle between $\boldsymbol{U}$ and the y-axis, and ϕ is the angle between the y-z plane and that containing $\boldsymbol{U}$ and the y-axis (for encounters at the ascending node $-\pi/2 < \phi < \pi/2$).

In Fig. 1 the velocity vectors are $\boldsymbol{U} = CP$ and $\boldsymbol{U}' = CQ$; θ and θ' are the angles between the y-axis and, respectively, $\boldsymbol{U}$ and $\boldsymbol{U}'$; ϕ and ϕ' are those between the y-z plane and, respectively, $\boldsymbol{U}$ and $\boldsymbol{U}'$; ψ is the angle between the planes $\boldsymbol{U}$-y and $\boldsymbol{U}$-$\boldsymbol{U}'$, and finally γ is the angle between $\boldsymbol{U}$ and $\boldsymbol{U}'$.

The modulus of $\boldsymbol{U}$ is:

$$U = \sqrt{3 - T} \tag{4}$$

where T is the well known Tisserand parameter:

$$T = \frac{1}{a} + 2\sqrt{a(1 - e^2)}\cos i. \tag{5}$$

Note that, computing the encounter velocity in this way, we are implicitly putting the heliocentric velocity of the planet $v_p = 1$, instead of $v_p = \sqrt{1 + m}$, where m is the mass of the planet.

The expressions of the components of $\boldsymbol{U}$ in terms of a, e and i are:

$$U_x = \pm\sqrt{2 - \frac{1}{a} - a(1 - e^2)} \tag{6}$$

$$U_y = \sqrt{a(1 - e^2)}\cos i - 1 \tag{7}$$

$$U_z = \pm\sqrt{a(1 - e^2)}\sin i \tag{8}$$

and those of a, e and i in terms of the components of $\boldsymbol{U}$ are:

$$a = \frac{1}{1 - U^2 - 2U_y} \tag{9}$$

$$e = \sqrt{U^4 + 4U_y^2 + U_x^2(1 - U^2 - 2U_y) + 4U^2 U_y} \tag{10}$$

$$i = \arctan \frac{U_z}{1 + U_y}; \tag{11}$$

in Eq. (6) the minus sign must be used for pre-perihelion encounters, and in Eq. (8) for encounters at the descending node.

These relations are valid for any orbit intersecting that of the planet, and thus, in particular, both for the pre-encounter and for the post-encounter orbit. In Öpik's theory the latter is obtained from the former in this way: the particle is assumed to move *unperturbedly* along the pre-encounter heliocentric orbit until it reaches the minimum distance from the planet b (the *impact parameter*); at that point $\boldsymbol{U}$ is rotated, by the *deflection angle* γ, into $\boldsymbol{U}'$, and the post-encounter orbital parameters a', e' and i' can then be computed, taking into account that $|\boldsymbol{U}'| = |\boldsymbol{U}|$, at the level of the approximations used.

Thus b is the distance between the planet and the intersection of $\boldsymbol{U}$ with the plane perpendicular to $\boldsymbol{U}$ containing the planet (the *b-plane*); γ, besides being the angle between $\boldsymbol{U}$ and $\boldsymbol{U}'$, is also the angle between the asymptotes of the planetocentric hyperbola on which the particle would move if the presence of the Sun were ignored, and its magnitude is given by:

$$\tan \frac{\gamma}{2} = \frac{m}{bU^2} \tag{12}$$

where m is the mass of the planet. In terms of d, the minimum encounter distance along the *perturbed* trajectory, we have

$$\sin \frac{\gamma}{2} = \frac{m}{m + U^2 d}. \tag{13}$$

After computing γ, we still need to determine the direction of $\boldsymbol{U}'$; since gravity is attractive, the direction of rotation is opposite, in the b-plane, to that joining the planet to the point of intersection between $\boldsymbol{U}$ and the b-plane itself. If ψ is, as said before, the angle between the planes $\boldsymbol{U}$-y and $\boldsymbol{U}$-$\boldsymbol{U}'$, and χ the angle between the planes $\boldsymbol{U}$-y and $\boldsymbol{U}'$-y, we can determine θ' and ϕ', the two angles defining the direction of $\boldsymbol{U}'$ (note that $\chi = \phi - \phi'$), by:

$$\cos\theta' = \cos\theta\cos\gamma + \sin\theta\sin\gamma\cos\psi \tag{14}$$

$$\tan\chi = \frac{\sin\psi\sin\gamma}{\cos\gamma\sin\theta - \sin\gamma\cos\theta\cos\psi} \tag{15}$$

$$\tan\phi' = \frac{\tan\phi - \tan\chi}{1 + \tan\phi\tan\chi} \tag{16}$$

thus being able, given the initial orbital elements a, e, i, and the parameters of the encounter, i.e. b (or d) and ψ, to compute the final values a', e' and i'.

The above formulae can be used to investigate the effects, on the outcomes of close encounters, of changing the mass of the perturbing planet; however, before doing this we can make some geometrical considerations useful to visualize the main features of the problem.

Let us start from Eq. (12), which gives the deflection angle γ as a function of m, the mass of the planet, b, the unperturbed miss distance, and U, the unperturbed planetocentric velocity of the particle.

The maximum possible deflection allowed by (12) is obviously $\gamma = 180°$, corresponding to the intuitively simple case in which the incoming velocity vector is exactly reversed, and this leads to a final orbit that, if the particle passes close enough to the planet, is essentially independent of the detailed geometry of the encounter, and can be easily computed from the formulae given above. Therefore, as noted by Valsecchi (1992a), we can associate to every incoming orbit a *conjugate* orbit, obtained by reversing the direction of $\boldsymbol{U}$ by 180°.

Since (2) and (9) imply that:

$$\frac{1}{a} = 1 - U^2 - 2U\cos\theta, \tag{17}$$

and U is constant, then a depends only on $\cos\theta$, i.e. on the projection of $\boldsymbol{U}$ along the direction of the planet's velocity; the variation of the specific orbital energy $E = -1/a$ (throughout this paper, we disregard the factor $1/2$ that should be present in the expression for E) is therefore given by:

$$\Delta E = \frac{1}{a} - \frac{1}{a'} = 2U(\cos\theta' - \cos\theta). \tag{18}$$

From this relation between a, U and θ follows that, for a given U, there are a minimum and a maximum possible value of the post-encounter specific orbital energy

$$E'_{min} = U^2 - 1 - 2U \tag{19}$$

$$E'_{max} = U^2 - 1 + 2U \tag{20}$$

that are obtained when, respectively, $\theta' = 180°$ and $\theta' = 0°$.

An interesting consequence of the geometry just described is that, unless $\theta = 0°$ or $\theta = 180°$, because of (18) the energy perturbation is larger for some not-so-small values of the impact parameter b – and suitably chosen ψ – than for infinitesimal b; this happens because in general the specific orbital energy of the conjugate orbit is different from either E'_{min} or E'_{max}, and only for the two orbits with $\theta = 0°$ and $\theta = 180°$, that are conjugate with each other, the energy difference is the maximum possible one.

Another consequence of (18), illustrated by Carusi et al. (1990), is the explanation of the asymmetric tails of cometary orbital perturbation distributions found by Everhart (1969) and Oikawa and Everhart (1979): if, for instance, the pre-encounter orbit has $\theta < 90°$, then $\cos\theta > 0$, and there are more possible end states of *lower* orbital energy (those with $-1 < \cos\theta' < \cos\theta$) than of *higher* orbital energy (those with $\cos\theta < \cos\theta' < 1$), i.e. the energy perturbation distribution must exhibit an excess of negative perturbations. The opposite obviously holds for $\theta > 90°$, and a perfectly symmetrical energy perturbation distribution can be expected only if $\cos\theta = 0$.

In general, if the encounter characteristics are such that $\gamma > 60°$, the change of velocity, given by:

$$|\Delta \boldsymbol{U}| = |\boldsymbol{U}' - \boldsymbol{U}| = 2U \sin \frac{\gamma}{2} \tag{21}$$

becomes larger than U, with the maximum $|\Delta \boldsymbol{U}| = 2U$ reached when $\gamma = 180°$; when this last situation is approached, $\boldsymbol{U}'$ tends towards the velocity vector corresponding to the conjugate orbit, and this has consequences on the perturbation distributions. In terms of the encounter parameters, the condition $|\Delta \boldsymbol{U}| = U$, beyond which we can expect that the influence of the geometry of rotation of the velocity vector becomes really evident, implies:

$$2|\sin \frac{\gamma}{2}| = \frac{2 \tan \frac{\gamma}{2}}{\sqrt{1 + \tan^2 \frac{\gamma}{2}}} = \frac{2m}{\sqrt{b^2 U^4 + m^2}} = 1. \tag{22}$$

However, the knowledge of the initial values of U and a allows us to say something more on the energy perturbation distribution; in fact, from (19) and (20) and the knowledge of the initial θ we can deduce that the *positive* tail of the energy perturbation distribution starts to exhibit a pathological behaviour (because closer encounters do *not* lead to larger energy perturbations) when

$$\theta = \gamma = 2 \arctan \frac{m}{bU^2} \tag{23}$$

and that the *negative* tail does so when

$$180° - \theta = \gamma = 2 \arctan \frac{m}{bU^2}. \tag{24}$$

Thus, for the same set of initial conditions, implying the same distribution of pre-encounter b and U, but different values of m, we expect the energy perturbation distributions to change shape at specific values of $|\Delta E|$, that depend only on the initial conditions and not on the planetary mass.

To illustrate in practice this point, we have computed large numbers of encounters with Neptune using Öpik's theory; for each encounter we have fixed the semimajor axis a of the initial orbit of the comet at 50 AU, and have chosen at random:

- the perihelion distance, so that $20 < q < 30$ AU;
- the cosine of inclination, so that $0.95 < \cos i < 1$;
- the coordinates b_ξ and b_ζ in the b-plane (see Appendix A), so that $-0.1 < b_\xi, b_\zeta < 0.1$, in units of the semimajor axis of Neptune.

This experimental set-up is intended to model *à la Öpik*, for unperturbed miss distances up to 3 AU, the starting conditions of the integrations of a disc-like cometary source done by Quinn et al. (1990). Actually, the initial orbital distributions change, after some time, in a way that is not deducible a priori (this is the very reason for performing numerical integrations!); here we are just trying to reconstruct the perturbation distributions *at the start* of Quinn et al.'s integrations.

The experiment has been performed, with identical initial conditions, for values of μ of 1, 10 and 40, corresponding to those used by Duncan et al. (1988) and by Quinn et al. (1990); the results are summarized in the left box of Fig. 2, which is a log-log plot of the frequency of perturbations N versus their absolute value $|\Delta E|$, in units of Neptune's specific orbital energy, done separately for positive and negative perturbations. We have also repeated the computations for initial conditions corresponding to the isotropic source of Quinn et al. (1990), allowing the cosine of the inclination to vary between 0 and 1, and the results of this second set of experiments are given in the right box of Fig. 2.

The fact that our curves exhibit maxima for not-so-small values of the perturbation is due to the upper limit we imposed on the miss-distance; above that limit the use of Öpik's theory, which assumes a point-like interaction, would be questionable. Actually, strict compliance with Öpik's prescriptions for the radius of applicability of his algorithm would have given a smaller upper limit, especially for $\mu = 1$; however, the results of the numerical integrations that we describe in the next section show that our upper limit is apparently still within the range of validity of Öpik's theory. In any case, the small distant perturbations, that if taken into account by the model would shift the maxima to the left, towards smaller values, are not of interest here, since the distortion of the distributions for increasing μ appears for the largest perturbations.

Let us first discuss the distributions for the disc-like source (left box of Fig. 2). For $\mu = 1$ the positive and negative energy perturbation distributions are very similar for $\log |\Delta E| \lesssim -1.5$, with some excess of negative perturbations starting to show up thereafter, and becoming significant for $\log |\Delta E| \gtrsim -1$. This asymmetry is a natural consequence of the choice of initial conditions, in view of the previous discussion of Eq. (18), since the energy perturbation distribution is symmetrical only if $\cos \theta = 0$.

The latter condition is shown in the left box of Fig. 3, which is a $\cos i$-q plot, where the continuous line joins the points for which $\cos \theta = 0$, given $a = 50$ AU. Our initial orbits, like the starting ones of Quinn et al. (1990), are evenly distributed in $\cos i$-q, and in the figure those to the upper right of the curve have $\cos \theta > 0$; thus, the sample corresponding to the disc-like source, that in the figure occupies the region above the dotted horizontal line at $\cos i = 0.95$, has to show a negative perturbation excess.

The right box of Fig. 3 illustrates another important difference between the two samples, i.e. the distribution of Tisserand parameter T, and hence of encounter velocity U, because of (4); for the disc-like source we have $2.56 < T < 2.97$ and $0.19 < U < 0.66$, while for the isotropic source we have $0.60 < T < 2.85$ and $0.39 < U < 1.55$, i.e. generally faster, less effective encounters.

Coming back to the perturbation distributions for the disc-like source, we see that for $\mu = 10$ the negative perturbation excess is significant already at the immediate right of the maxima of the pair of curves, meaning that even for distant encounters, those with $b \approx 2 \div 3$ AU, the perturbation asymmetry is at work. For $\mu = 40$ the maxima move further to the right, towards $\log |\Delta E| \approx 0.15$; this value is close to the maximum possible perturbation for our set of initial orbits and so, not surprisingly, in its vicinity the curves have to bend downwards. Going be-

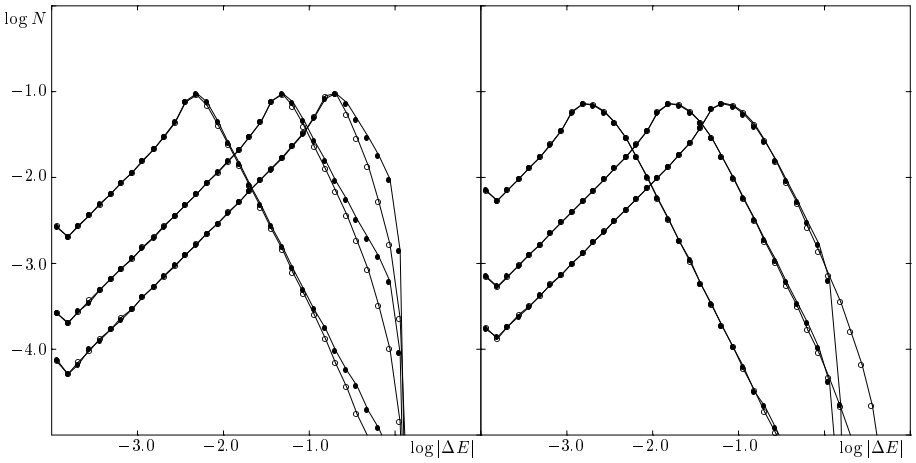

Fig. 2. Frequency of energy perturbations vs. their absolute value for comets interacting with Neptune, according to Öpik's theory; the initial conditions for the left box are the same as those of disc-like source of Quinn et al. (1990), and those for the right box are the same as those of isotropic source of the same authors. The three pairs of curves in each box correspond, left to right, to μ = 1, μ = 10, and μ = 40; the distributions of positive perturbations are denoted by open dots, those of negative perturbations by full dots. The units on the vertical axis are normalized to the total number of encounters for each value of μ.

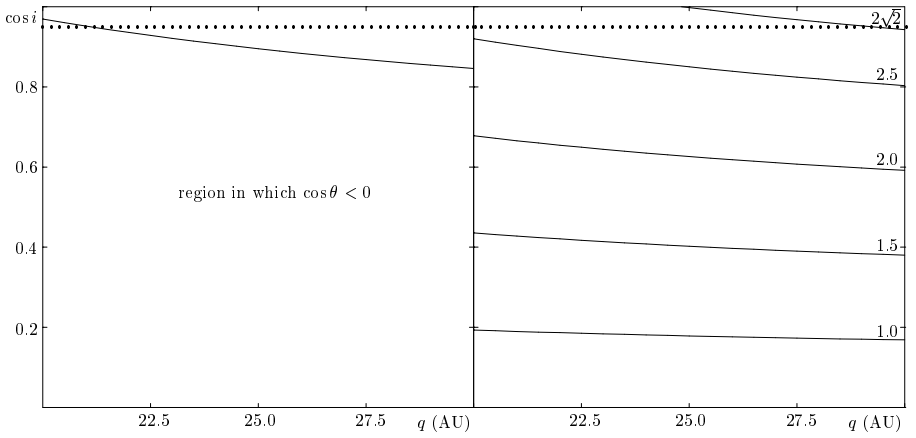

Fig. 3. Left: the condition $\cos\theta = 0$ in the $\cos i$-q plane; orbits to the upper right of the curve have $\cos\theta > 0$. The starting orbits of Quinn et al. (1990) for a disc-like source are evenly distributed above the horizontal dotted line corresponding to $\cos i$ = 0.95, whereas those for an isotropic source are evenly distributed in the entire range shown in the figure. Right: the conditions $T = 2\sqrt{2}$, T = 2.5, T = 2, T = 1.5, T = 1, in the same plane.

yond μ = 40 we would see an even more pathological behaviour, with the perturbation distributions being squeezed against the condition $\log|\Delta E| \approx 0.15$. Incidentally, let us note that for $\mu \gtrsim 29$, according to Nacozy (1976), the hierarchy of the triple system Sun-Jupiter-Saturn would be broken in less than a few thousand years, and Saturn would be ejected from the system, if the planets were allowed to perturb each other.

The perturbation distributions of the isotropic source, however, behave in a different way with increasing μ, as shown in the right box of Fig. 2. Actually, there is no asymmetry for values of $\log|\Delta E|$ up to about -1; beyond this value, and up to $\log|\Delta E| \approx 0$, negative perturbations dominate, while for larger values of $|\Delta E|$ positive perturbations largely outnumber the negative ones. It is noteworthy that the latter regime, the one in which positive large energy perturbations are prevalent, is only recognizable for large μ, since for μ = 1 it would require extremely close, and thus extremely rare, close encounters.

The key to understand what is going on is given by Eqs. (17), (19) and (20): since all our orbits have the same a and the same distribution of q, but different distributions of i, we have that the isotropic source extends to lower values of T, i.e. larger values of U, and to smaller values of $\cos\theta$ (see Eq. 17 and Fig. 3); this in turn means that, because of Eq. (20), larger and larger *positive* ΔE_{max} become accessible, as i increases, whereas the same is not true for *negative* ΔE_{max}, due to the form of Eq. (19).

Fig. 4 illustrates what we have just described; it shows the condition $\log|\Delta E_{max}|$ =const. for negative (left box) and positive energy perturbations (right box). For the disc-like source (above the dotted line), the maximum negative values of ΔE are somewhat larger than the maximum positive ones and in addition, as already seen before, the majority of orbits have $\cos\theta > 0$, so that negative large perturbations are more numerous than positive large ones.

For the isotropic source, negative values of initial $\cos\theta$ largely dominate, so that one would expect that the asymmetry of large perturbations to be in favour of the positive ones; however, the fact that the values of $\log|\Delta E_{max}|$ for negative perturbations level off slightly beyond $\log|\Delta E| \approx 0.14$ implies that deep decelerating encounters in a vast region of the q-i space all contribute to the perturbation bins approaching this value, causing the excess of negative perturbations noted before. Going to larger perturbations, however, the positive tail of the perturbations "owns the battlefield", as expected.

We have thus seen that the effect of $\mu \gtrsim 10$, in the case of initially crossing orbits, is to alter the distribution of energy perturbations by significantly varying the proportion of positive and negative *large* perturbations with respect to the case of μ =

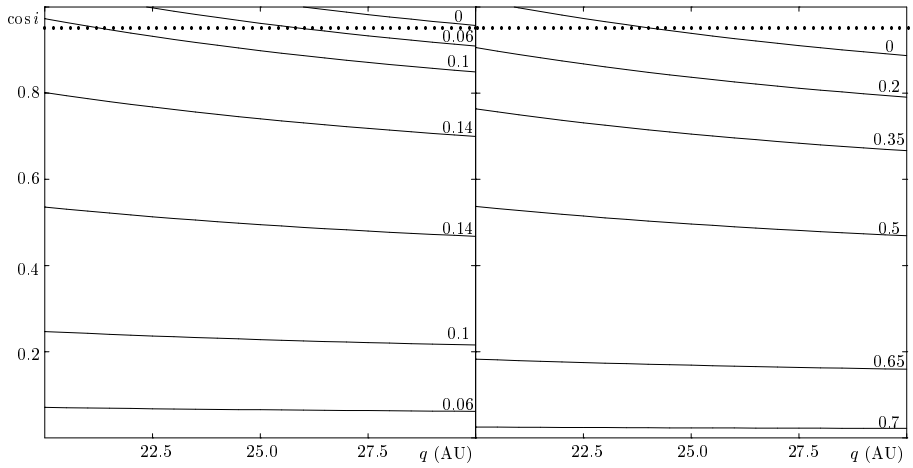

Fig. 4. Left: the conditions $\log|\Delta E_{max}| = 0$, $\log|\Delta E_{max}| = 0.06$, $\log|\Delta E_{max}| = 0.1$, $\log|\Delta E_{max}| = 0.14$, in the $\cos i$-q plane, for *negative* energy perturbations.
Right: the conditions $\log \Delta E_{max} = 0$, $\log \Delta E_{max} = 0.2$, $\log \Delta E_{max} = 0.35$, $\log \Delta E_{max} = 0.5$, $\log \Delta E_{max} = 0.65$, $\log \Delta E_{max} = 0.7$, in the same plane, for *positive* energy perturbations.

1; to avoid this μ should be kept in the vicinity of 1, but in this case, of course, the very reason for using $\mu > 1$, i.e. to obtain a significant speed-up of the numerical integrations, would be lost.

3. Numerical checks

To verify that the shape of the perturbation distribution does indeed change when the planetary masses are enhanced, we have performed various sets of numerical integrations characterized by the same initial conditions but different values of μ. The integrations were done with the same program of Manara and Valsecchi (1991) – based on the RADAU integrator (Everhart 1985) – but having only Neptune, on a circular orbit, as perturber, and using for the fictitious comets the same distribution of initial conditions of Quinn et al. (1990). Each comet has been followed for a time span corresponding to one sidereal period computed from the initial value of a (equal to 50 AU for all of them), i.e. for about 354 yr. We obtained the ΔE distributions simply from the difference between the value of $E' = -a_N/a'$ at the end of the one-revolution integration and the starting one, $E = -a_N/50$. A total of 100 000 comets was integrated for each value of μ.

Fig. 5 shows the distributions that we obtained, for $\mu = 1$, $\mu = 10$ and $\mu = 40$, for both sources, when we limited the integrations to the cases in which the miss distance b, computed along the unperturbed orbit, was less than 3 AU, in order to be able to compare with the results of Öpik's theory; this procedure made up for very long computations, since a very large number of orbits had to be followed unperturbedly in order to extract the 100 000 necessary to draw each pair of curves.

The overall agreement of Fig. 5 with Fig. 2 is remarkable. For the disc-like source the squeezing of the distributions, as μ increases, against the condition $\log|\Delta E| \approx 0.15$, as well as the prevalence of negative large perturbations, are well reproduced; the same can be said for the features of the distributions related to the isotropic source, with the negative perturbations being more abundant for $\log|\Delta E|$ approaching 0.1 and positive perturbations largely dominating thereafter, and by much wider margins for larger μ.

We repeated the same numerical experiments dropping the condition $b \leq 3$ AU, in order to see how much of the alterations of the distributions for $\mu > 1$ would be still present when the strong perturbations due to close encounters are "diluted", as it happens in reality, by the much more numerous weak, ordinary perturbations. Fig. 6 shows the distributions that we obtained in this way.

In this case for both sources the largest values of $\log|\Delta E|$ obtained with $\mu = 1$ are smaller than the thresholds beyond which the asymmetries become noticeable. On the other hand, for $\mu \geq 10$ a sufficient number of large perturbations is present in the samples so as to clearly show, for the disc-like source, the negative large perturbations excess, therefore indicating a qualitative difference with the almost-asymmetry-free perturbation distribution characterizing the $\mu = 1$ case shown in the figure. For the isotropic source, the positive large perturbation excess for large μ is reproduced, whereas the negative excess for less extreme perturbations is recognizable only for $\mu = 40$.

Overall, Fig. 6 confirms the distortions of the distributions introduced by $\mu \geq 10$, and shows that they are especially significant for the disc-like source, where the squeezing imposed by the geometrical constraints on the rotation of the planetocentric velocity vector is recognizable even on the relatively small perturbation samples shown in the figure.

4. Encounters on nearly-tangent orbits

A substantial fraction of planetary encounters undergone by comets takes place on nearly-tangent orbits. Manara and Valsecchi (1991), integrating fictitious objects in low-eccentricity, low-inclination orbits in the outer planetary region, found about 30% of the encounters to be of this type. For observed short-period comets these encounters are also rather frequent, as can be seen in the catalogues of orbital evolutions of Carusi et al. (1985, 1995) and Belyaev et al. (1986).

As a matter of fact, Öpik's theory cannot be applied when the orbits are not crossing, and in this case the encounters must be treated in the framework of a more-than-two-body-problem. Nevertheless, many of the short-period comets discovered in the last few decades have undergone such encounters with Jupiter,

and their evolutions have been studied numerically in detail, so that some qualitative understanding of the main features of these encounters has been obtained.

Good examples of encounters with Jupiter on nearly-tangent orbits are those of 39P/Oterma, between 1933 and 1941, and of 82P/Gehrels 3 between 1963 and 1976. In both cases the initial orbits were well decoupled from that of Jupiter (Carusi et al. 1985, 1995), since the pre-encounter perihelion distances were large, $q \approx 5.7$ AU, and the inclinations very low, $i \approx 3°$, so that the Tisserand parameter T (computed with respect to Jupiter) was greater than 3 and no encounter velocity U could be computed; the final aphelia were well inside Jupiter's orbit, $Q \approx 4.5$ AU.

In this type of encounters the comet's approach is from the front, if its semimajor axis is greater than that of the planet, or from behind, in the other case, with the planetocentric velocity vector respectively nearly anti-parallel (or nearly parallel) to the direction of motion of the planet; after some time spent in the vicinity of the planet, during which a temporary satellite capture is possible, the comet leaves that region either with essentially the same incoming velocity or with the planetocentric velocity rotated by about 180°. In the first case the final semimajor axis is close to the initial one, and in the second it has jumped to one lower than that of the planet, if the initial one was larger, or vice-versa.

This last case resembles the one, discussed in Sect. 2, of the 180° deflection of the velocity vector into the conjugate orbit; however, to the deflection into the conjugate orbit can correspond any value of the energy perturbation, depending on the initial θ, and in particular even a null energy perturbation, when $\theta = 90°$, while in the present case the perturbation, when the velocity vector is reversed, is about twice the difference between the specific orbital energy of the comet and that of the planet. This is shown by Fig. 8 of Carusi et al. (1981), where is given the distribution of $-1/a$ perturbations for 79 fictitious objects, plus the real 39P/Oterma, for the 1933-1941 nearly-tangent encounter mentioned before: the histogram has two peaks, at 0 and at -0.1 AU^{-1}, with nothing in between.

We can get an estimate of how the perturbation distributions in these encounters scale with μ by considering the size and shape of Hill's surfaces of zero velocity in the restricted circular three-body problem. When these surfaces are nearly closed, for $T \gtrsim 3$, in order to encounter the planet the comet has to pass close to one of the Lagrangian points L_1 and L_2, depending on whether it comes from an exterior or an interior orbit. The approach to the Lagrangian point is slow, and becomes even slower when the comet reaches the immediate vicinity of the point. We then compute the orbital elements of the comet *at* the Lagrangian point, with zero velocity relative to it: in fact, since most of the orbital perturbation takes place when the comet is at a distance from the planet smaller than that of the Lagrangian points, we can assume these elements as typical of the pre-encounter and post-encounter orbits.

The distance h of L_1 and L_2 from the planet, in units of its semimajor axis, is:

$$h \simeq \sqrt[3]{\frac{m}{3}} \tag{25}$$

where m, as before, is the planet's mass in units of that of the Sun. The comet, when at rest in L_1 would then be at the perihelion of a heliocentric orbit with $q = a(1-e) = 1+h$, and when at rest in L_2 would be at the aphelion of a heliocentric orbit with $Q = a(1+e) = 1-h$; in both cases $i = 0$.

To obtain a and e of these orbits we compute the comet's heliocentric velocity v:

$$v^2 = (1+h)^2 = \frac{2}{1+h} - \frac{1}{a} \tag{26}$$

for the comet in L_1, and

$$v^2 = (1-h)^2 = \frac{2}{1-h} - \frac{1}{a} \tag{27}$$

for the comet in L_2 (as before we disregard the difference from unity of the planet's velocity); keeping only the first power of h we get

$$a \simeq \frac{1+h}{1-3h} \tag{28}$$

for the comet in L_1, and

$$a \simeq \frac{1-h}{1+3h} \tag{29}$$

for that in L_2, with

$$e \simeq 3h \tag{30}$$

in both cases. For Jupiter, that means $e \simeq 0.2$, and $a \simeq 7$ AU, for a comet coming from, or ending in, an exterior orbit, and $a \simeq 4$ AU in the other case. These estimates are in good agreement, given the crudeness of the argument, with the pre-encounter and post-encounter orbits of 39P/Oterma ($a = 6.92$ AU, $e = 0.16$ and $a = 3.98$ AU, $e = 0.15$) and of 82P/Gehrels 3 ($a = 6.94$ AU, $e = 0.18$ and $a = 4.05$ AU, $e = 0.15$), indicating that the pre- and post-encounter sizes and shapes of the orbits depend essentially on the size of h and, therefore, on the mass of the planet. This agrees with the results found in an analysis of the motion of comets undergoing encounters of this type by Tancredi et al. (1990), who proceeded along a similar way of reasoning, taking also into account the eccentricity of Jupiter's orbit.

We then compute the specific orbital energy difference between the two Lagrangian points

$$E_{L_1} - E_{L_2} \simeq \frac{1+3h}{1-h} - \frac{1-3h}{1+h} \simeq 8h \tag{31}$$

in this way obtaining the distance between the two peaks in the perturbation distribution. For Jupiter $8h \simeq 0.5$, in units of the

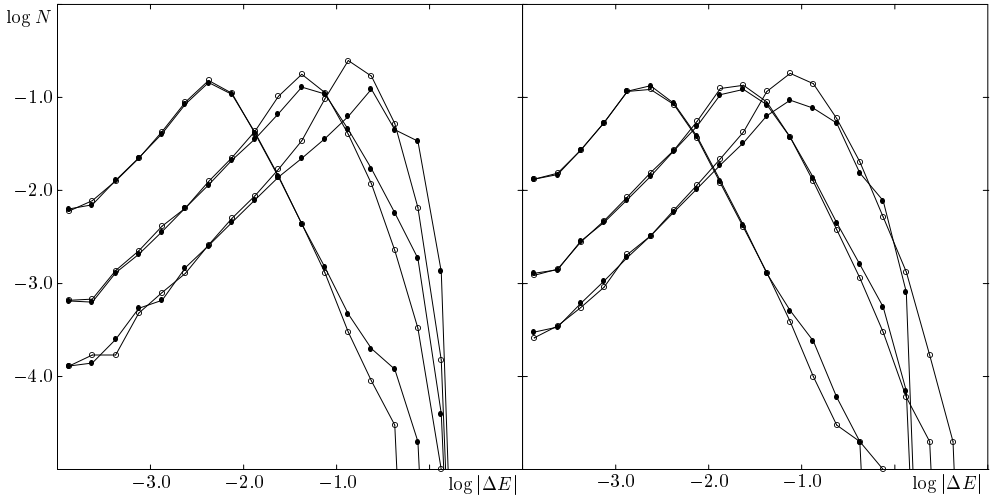

Fig. 5. Frequency of energy perturbations vs. their absolute value for comets interacting with Neptune, from numerical integrations; in this figure, only perturbations characterized by $b \leq 3$ AU are taken into account. The left box refers to the disc-like source, the right one to the isotropic source; the distributions are arranged as in Fig. 2.

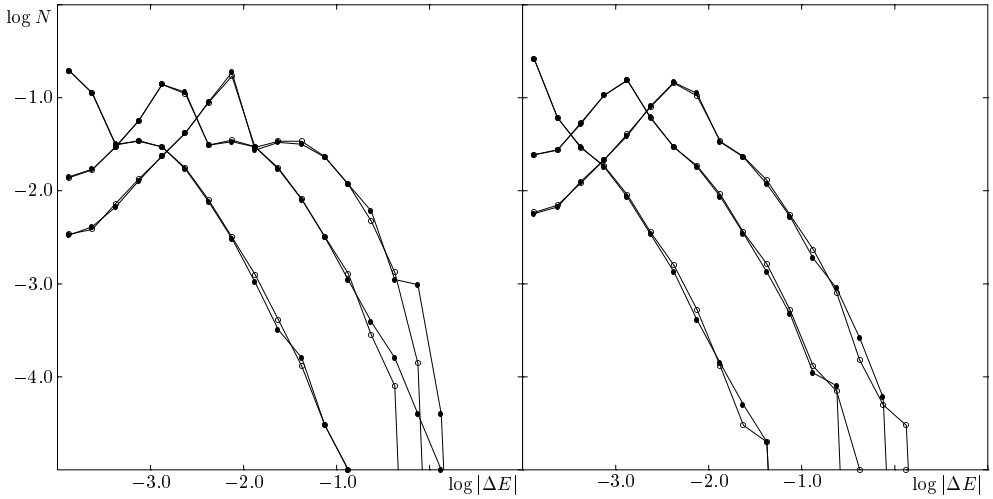

Fig. 6. Same as Fig. 5, but dropping the condition $b \leq 3$ AU.

planet's specific orbital energy; expressed in AU^{-1}, this value agrees well with the result by Carusi et al. (1981).

Thus, also in the case of nearly-tangent encounters, which is not treatable with Öpik's theory, the enhancement of the masses of the perturbing planets affects the energy perturbation distributions, but in a way which is different from what we obtained in the case of crossing orbits. The altered distribution remains bimodal, like that found by Carusi et al. (1981), with one peak centred on 0, but the distance between the peaks varies with $\sqrt[3]{\mu}$.

5. Dynamical paths in the outer planetary region

To illustrate the consequences of the results of the last section, let us consider Fig. 7, which is an E-e plot of the solar system. In the left box of this figure the four pairs of straight lines starting at $e = 0$ refer, top to bottom, to Neptune, Uranus, Saturn and Jupiter respectively, and represent orbits for which either $q = a_p$ (upper line of each pair, a_p is the planet's semimajor axis) or $Q = a_p$ (lower line); orbits that are within the pair of lines of a planet can cross the orbit of the latter. Also shown in the left box of the figure, as small dots, are the orbits, computed for $\mu = 1$, corresponding to the small body at rest in the Lagrangian points L_1 and L_2, whose semimajor axes and eccentricities have been given in Sect. 4. In the central and right boxes of the figure there are the same lines and dots, but with the positions of the latter computed for $\mu = 10$ and $\mu = 40$ respectively.

Comets close to these orbits can jump from inside to outside, or vice-versa, of the orbit of the corresponding planet, and the dots shown in Fig. 7 can be therefore considered to be the milestones of the cometary dynamical path, consisting of nearly-tangent orbits, long-known from studies of the past evolutions of observed short-period comets. As the central and right boxes of Fig. 7 show, these milestones are shifted towards larger eccentricities for $\mu = 10$ and $\mu = 40$, and those relative to Jupiter and Saturn are in regions in which crossing encounters with adjacent planets are possible, something not allowed for $\mu = 1$. In this way new dynamical paths are open, like for example transitions from a Uranus-crossing to a Saturn-tangent orbit, and only the detailed examination of intermediate stages of numerical integrations can tell us what is their actual impact on the overall evolution.

In order to discuss more in general the evolution of cometary orbits in the outer planetary region let us now examine, in Fig. 8, various views of a relevant parameter space first introduced by Kresák (1972, 1982).

Table 1. Orbital elements, specific orbital energies and Tisserand parameters with respect to each outer planet of the known Centaurs.

Asteroid		i	e	a	$-a_J/a$	T_J	$-a_S/a$	T_S	$-a_U/a$	T_U	$-a_N/a$	T_N
(2060) Chiron	1977 UB	6.9	0.383	13.699	−0.38	3.36	−0.70	2.89	−1.41	2.95	−2.21	3.45
(5145) Pholus	1992 AD	24.7	0.572	20.295	−0.26	3.20	−0.47	2.64	−0.95	2.48	−1.49	2.71
	1993 HA_2	15.6	0.522	24.735	−0.21	3.79	−0.39	3.03	−0.78	2.64	−1.22	2.71
	1994 TA	5.4	0.306	16.818	−0.31	3.72	−0.57	3.08	−1.15	2.92	−1.80	3.21
	1995 DW_2	4.1	0.246	25.030	−0.21	4.45	−0.38	3.51	−0.77	2.97	−1.21	2.97
	1995 GO	17.6	0.622	18.126	−0.29	3.07	−0.53	2.58	−1.06	2.51	−1.67	2.83

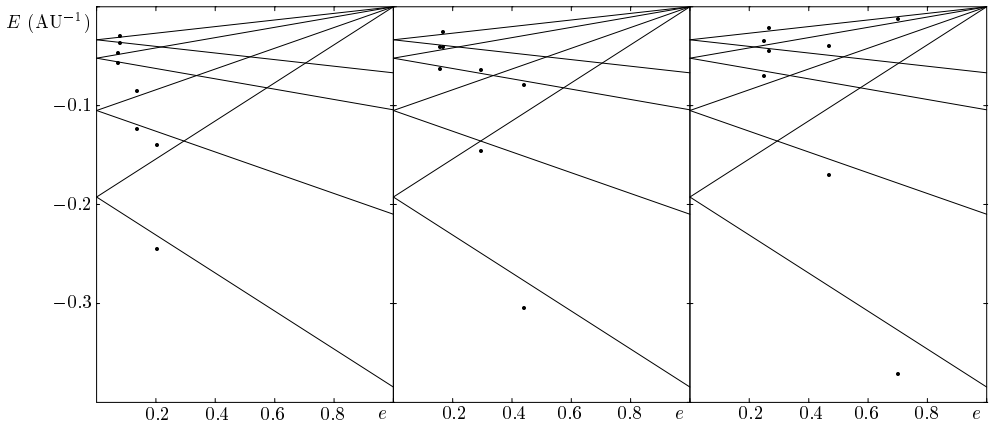

Fig. 7. E-e plot of the solar system. In each of the three boxes of the figure the tangency conditions for each of the four outer planets are shown and the dots denote orbits corresponding to the Lagrangian points L_1 and L_2 of each planet; the left plot is for $\mu = 1$, the central one for $\mu = 10$ and that on the right for $\mu = 40$.

In the top plot of the figure the dots denote all the periodic comets contained in Marsden and Williams' Catalogue of Cometary orbits (1992), as well as all the long-period comets, taken from the same catalogue, for which original orbits have been computed, while the open circles denote all the Centaurs and trans-neptunian objects currently known, taken from the listings available at the Minor Planet Center World Wide Web server; they are plotted in a $-a_J/a$ vs. $-T_J$ diagram, where a_J is the semimajor axis of Jupiter's orbit and T_J is the Tisserand parameter evaluated with respect to this planet:

$$T = \frac{a_J}{a} + 2\sqrt{\frac{a(1-e^2)}{a_J}}\cos i. \tag{32}$$

The three other plots, containing the same objects, have as axes $-a_S/a$ vs. $-T_S$, $-a_U/a$ vs. $-T_U$ $-a_N/a$ vs. $-T_N$, i.e. the specific orbital energy and the Tisserand parameter computed with respect to Saturn, Uranus and Neptune.

In each plot, vertical lines are drawn for values of the Tisserand parameter equal to 3, $2\sqrt{2}$ and 2. In general, for $T_p \gtrsim 3$ (where p can be J, S, U or N) comets have dynamical characteristics like those of 39P/Oterma (very slow encounters, with the possibility of perihelion-aphelion exchanges and temporary satellite captures); for $3 \gtrsim T_p \gtrsim 2\sqrt{2}$ direct ejection into hyperbolic orbit due to an encounter with planet p is impossible, while for lower values of T_p these ejections become possible. Finally, for $T_p < 2$ the encounter velocity becomes larger than the orbital velocity of the planet; in the case of Jupiter, $T_J < 2$ is becoming widely used to separate Halley-type comets from Jupiter-family ones, following the suggestion by Carusi et al. (1987; see also Kresák 1994, Levison and Duncan 1994, and Valsecchi 1992b).

The curve on the left of each plot corresponds, for $i = 0$, to circular orbits; it delimits a forbidden region, since at its left $e^2 < 0$. Along the curve, arrows denoted by letters point to the positions of the planets whose name begin with the corresponding letters; the planet whose semimajor axis is used as unit of length is located at $-a_p/a = -1$ and $T_p = 3$. The curve tangent to the circular limit at the planet's position corresponds to orbits tangent to that of the planet in their perihelion (for $a > a_p$) or aphelion (for $a < a_p$); this curve and the circular limit are inclination dependent.

The 45°-inclined line from $-a_p/a = -1$, $T_p = 3$ to $-a_p/a = 0$, $T_p = 2$ corresponds to $\cos\theta = 0$; as we have seen before, above it the distribution of energy perturbations presents an excess of negative large perturbations, while below it the opposite is true. Finally, the other 45°-inclined line, the one from $-a_p/a = -2.5$, $T_p = -2.5$ to $-a_p/a = 0$, $T_p = 0$ corresponds to orbits for which the z-component of the angular momentum is null, i.e.:

$$\sqrt{\frac{a}{a_p}(1-e^2)}\cos i = 0; \tag{33}$$

for these orbits, fall into the Sun at an extreme of their ω-cycle is possible (Bailey et al. 1992).

Despite this long list of lines and curves, these plots make the task of understanding the evolution of cometary orbits somewhat easier; in fact, due to the approximate conservation of the

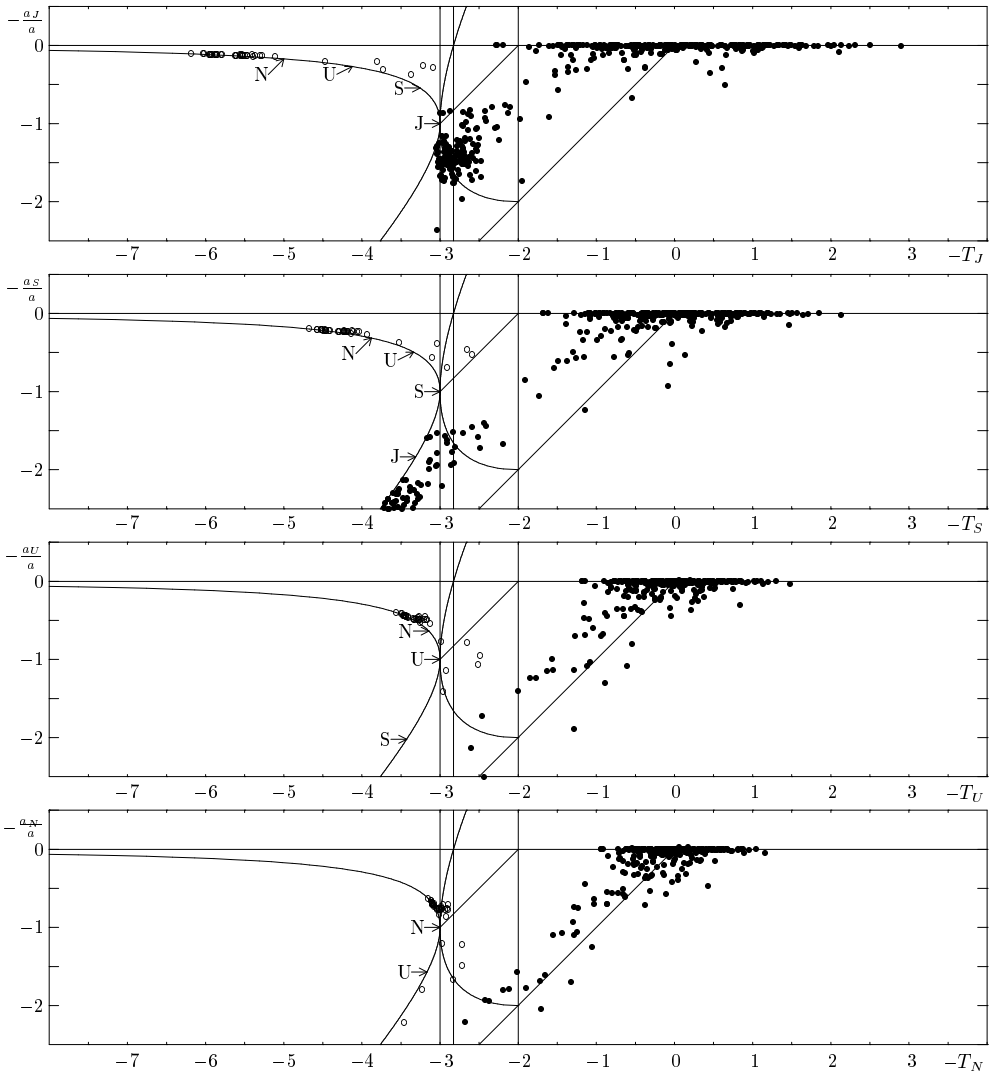

Fig. 8. Comets, Centaurs and trans-neptunian objects in a (top to bottom) $-a_J/a$ vs. $-T_J$, $-a_S/a$ vs. $-T_S$, $-a_U/a$ vs. $-T_U$ $-a_N/a$ vs. $-T_N$ diagram; for explanations, see the text.

Tisserand parameter relative to a certain planet at close encounters with that same planet, the evolution mostly takes place along straight lines.

If a comet suffers a large perturbation in energy due to, say, an encounter with Saturn, it is displaced along a vertical line (corresponding to its value of T_S) in the second plot from the top, the one relative to Saturn. In the other three plots, however, its displacement will be along a straight line parallel to the tangent to the circular limit *at Saturn's position* (this can be shown starting from the definition of T_p, see Appendix B); similar statements hold for encounters with the other major planets.

In this way one can relatively easily visualize the path along which objects starting from the Edgeworth-Kuiper belt can reach the region of Jupiter-family comets. To this purpose, let us examine in more detail, with the help of Fig. 9, the way in which former Edgeworth-Kuiper belt members (Trans-Neptunian Objects, TNOs) can pass from the dynamical control of Neptune to that of Uranus. This figure contains an enlargement of the third box from top of Fig. 8, the one centred on Uranus, and in it are reported not only the various curves referring to Uranus, but also those referring to Neptune, in order to illustrate the dynamical paths and the geometrical constraints on the orbits.

The currently known TNOs are characterized by $2.89 \leq T_N \leq 3.14$; those that reach a dynamical situation allowing close encounters with Neptune would do so with $2.9 \lesssim T_N \lesssim 3.0$, thus meaning that encounters with Neptune will be unable to eject them on hyperbolic orbits. In Fig. 9 we can see that the TNOs that are on more eccentric orbits, the ones in the $2/3$ mean motion resonance with Neptune, are characterized by the lowest values of T_N; their orbits cross already the orbit of Neptune, and would have close encounters with the planet if they lost the phase protection given by the resonance. The non-resonant TNOs, on the other hand, would more probably become able to encounter Neptune by reaching orbits nearly tangent to that of the planet, with $T_N \gtrsim 3$. Either way, once their dynamics is controlled by encounters with Neptune all these former TNOs would tend to move between the two lines $T_N = 3$ and $T_N = 2\sqrt{2}$; in a first phase they would have, relative to Neptune, $\cos\theta > 0$ (see Fig. 9, where the TNOs are above the line $\cos\theta = 0$ relative to that planet) so that the perturbation

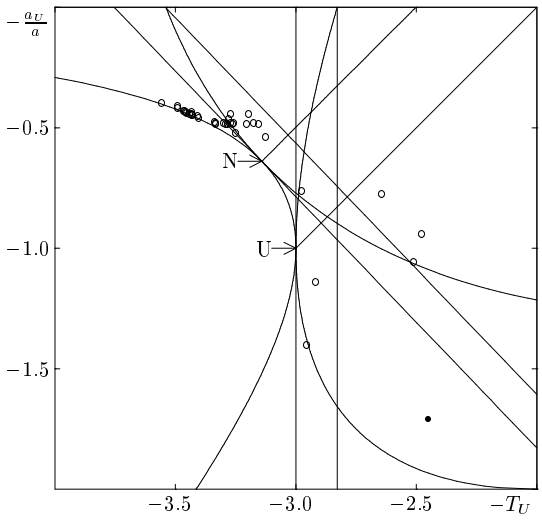

Fig. 9. An enlargement of the third box on the top of Fig. 8, the one relative to Uranus; for explanations, see the text.

distribution would have a negative excess, favouring a decrease of the orbital energy and thus a shrinking of the orbit. After some time the condition $\cos\theta = 0$ will be crossed, the sign of the asymmetry of the perturbation distribution will change and the further progress toward Uranus-controlled orbits will be slower, with many objects brought back at higher semimajor axes by very close encounters. Nevertheless, some objects will reach Uranus-tangent or Uranus-crossing orbits after a suitable sequence of decelerating perturbations.

It is then probable that those former TNOs that will be "passed on" to Uranus will have $2\sqrt{2} \lesssim T_U \lesssim 3.0$; to see this, let us consider that the T_N =const. lines in Fig. 9 cross the T_U =const. ones at a certain angle, and that very close encounters with Neptune on crossing orbits in a vast majority of cases would displace the bodies inwards only as far as the aphelion of the final orbit is not smaller than a_N, a condition shown in the figure. It is easy to see that only for the extreme negative perturbations, and for T_N tending towards $2\sqrt{2}$, the ex-TNO can end up in an orbit with $T_U < 2\sqrt{2}$.

Once in the "corridor" $2\sqrt{2} \lesssim T_U \lesssim 3.0$, similar considerations would apply to the further evolution towards Saturn-controlled orbits, and again the relatively high value of the Tisserand parameter with respect to the controlling planet would prevent hyperbolic ejections, thus making for an efficient transport process. Note that hyperbolic ejections *can* take place also for objects that at a certain point of their orbital evolution are in the "corridor" relative to planet p, but only if either their T_p becomes less than $2\sqrt{2}$ (see later for a discussion of the causes that can lead to this), or if they are ejected by another planet, say p', with respect to which $T_{p'} < 2\sqrt{2}$.

Considering the currently known Centaurs (see Table 1 for their orbital elements as well as for their specific orbital energies and Tisserand parameters with respect to the four outer planets), we have that three of them, namely Chiron, 1994 TA and 1995 DW_2, seem to fit the above scenario; on the other hand, the other three have much lower values of T_U.

This may have several reasons. First, we have neglected in this discussion the effect of planetary eccentricities on the conservation of the Tisserand parameter; according to Öpik (1976), the effect of repeated encounters with a planet on an eccentric orbit is to secularly decrease T. Second, and probably more important, the effect of close encounters with another planet can lead, as discussed before, to important variations of the Tisserand parameter with respect to the planet under consideration; to this purpose it is interesting to note that, of the three Centaurs with $T_U < 2\sqrt{2}$, 1993 HA_2 can interact with Uranus and Neptune, while Pholus and 1995 GO can interact with Saturn, Uranus and Neptune, thus increasing the chances for T_U to decrease over time.

It is then clear that an artificial increase of the energy perturbations in computations using larger planetary masses would enhance the effect just described and therefore, similarly to what discussed at the end of the previous section, it would lead to significantly different evolutionary routes; in particular, due to the lower values of T relative to the various controlling planets, these routes would allow a higher rate of losses to hyperbolic orbits.

6. Conclusions

In the previous sections we have shown that the shape of the energy perturbations distributions at close encounters depends on μ, the planetary mass enhancement factor used to speed-up numerical integrations of orbital evolutions.

In the case of crossing encounters we have used Öpik's theory; the validity of this theory in the present context is shown by the result of Carusi et al. (1990), who were able to reproduce the original result of Everhart (1969), whose integrations of cometary encounters with Jupiter showed the existence of asymmetric tails in perturbation distributions, and by the numerical checks done for this paper, in which we have computed the distribution of energy perturbations for the same initial conditions of the disc-like source of Quinn et al. (1990) using three different values of mass enhancement, namely $\mu = 1$, $\mu = 10$ and $\mu = 40$. These results refer to a set of *initial orbits* like to that used by Quinn et al. (1990), and so they do not necessarily apply to what happens to the orbits in the course of the numerical integrations. It is likely, however, that alterations in the first phases of the evolution introduced by using $\mu > 1$ would propagate to the successive phases.

The geometry involved in Öpik's theory is useful also to understand the greater efficiency of a disc-like over an isotropic source, which is a very important point in the Edgeworth-Kuiper-belt vs. inner-Oort-cloud debate. Referring to the left box of Fig. 3, we can see that the range of inclinations used by Quinn et al. (1990) for the computations starting from a prograde isotropic source spans the whole figure, and so most of the starting orbits have $\cos\theta < 0$, and thus positive perturbation excess, helping to explain the lower efficiency of this source.

No equivalent of Öpik's theory exists for the case of encounters on nearly-tangent orbits; we have presented an argument, based on the opening of the zero-velocity curves of the restricted, circular three-body problem, implying that the perturbation distribution is bimodal, with two well separated peaks – as shown by the numerical integrations by Carusi et al. (1981) – one of which is at about $|\Delta E| = 0$, with the other at $|\Delta E| = 8h(\mu)$, thus showing that also in this case the perturbation distribution depends on μ.

We have seen that the orbital evolution in the outer planetary region can be conveniently discussed in an orbital energy vs. Tisserand parameter diagram; one can expect that the multistage capture, in the case of the real masses of the outer planets, should take place along a low inclination path rather close to the circular limit in the diagram, and this implies that along this path the values of T_p relative to the planet controlling the motion should not become too much smaller than 3. For $\mu > 1$, on the other hand, the path should be displaced away from the circular limit, at lower values of T_p with respect to the controlling planets; if the values of T_p become at a certain stage less than $2\sqrt{2}$, hyperbolic ejections would become possible, thus decreasing the efficiency of the transfer process.

Finally, the orbital energy vs. Tisserand parameter diagrams also illustrate how little is the contribution that comets coming from the Oort cloud, directly perturbed by Jupiter into more tightly bound, observable orbits, can give to the Jupiter family: most of the *observed* long period comets have $T_J < 2$, and the perturbations of all the four giant planets simply do *not* work in the right direction to bring them into orbits of short period and $T_J > 2$ (Kresák 1982).

Acknowledgements. We are grateful to M. Bailey, J. Fernández, the late Ľ. Kresák and H. Rickman for useful discussions on the subject of the paper, and to M. Carpino, A. Carusi, P. Farinella, Ch. Froeschlé, Cl. Froeschlé, A. Morbidelli and E. Perozzi for critically reading the manuscript. GBV did part of the work described in this paper while holding the G. Colombo Fellowship of the European Space Agency.

Appendix A: setting up encounters in the *b*-plane

Given a set of initial orbital elements for bodies encountering a planet, i.e. given triples of a, e, i or equivalent elements, the next problem is that of appropriately choosing sets of values of b and ψ. If the set of initial orbits is composed of highly inclined deep crossers, then one may choose at random either simply b^2 between 0 and b^2_{max}, and ψ between 0 and 2π, or b_ξ and b_ζ (two orthogonal coordinates in the b-plane, see later for details) between $-b_{max}$ and b_{max}, discarding the cases in which $b^2_\xi + b^2_\zeta > b^2_{max}$; the latter method is the one we used, since it is easily adapted to the constraints described below. On the other hand, if among the initial orbits there are some that fulfill one or more of the following conditions

$$\sin i < b_{max} \tag{A1}$$
$$1 - b_{max} < q \tag{A2}$$
$$Q < 1 + b_{max} \tag{A3}$$

then one must consider the limitations to the coordinates in the b-plane coming from orbital geometry, since some combinations of b and ψ are not allowed.

In order to compute the appropriate boundaries, we note that (A1), (A2) and (A3) imply, respectively,

$$|b_z| < \sin i \tag{A4}$$
$$-b_{max} < b_x \tag{A5}$$
$$b_x < b_{max} \tag{A6}$$

where b_x, and b_z are the first and third component of $\boldsymbol{b}$ in the planetocentric rotating frame. Note that (A5) and (A6) can be combined into

$$-b_{max} < b_x < b_{max} \tag{A7}$$

allowing encounters on orbits with $1 < q < 1 + b_{max}$ or $1 - bmax < Q < 1$, something that can be done provided that, in such cases, care is taken in order to choose b and ψ only in the ranges allowed by orbital geometry, as we do.

In general, given the coordinates ξ, η, ζ of a point in the frame whose η-axis is directed along $\boldsymbol{U}$ and whose $\eta\zeta$-plane contains the direction of motion of the planet (this is the frame whose $\xi\zeta$-plane *is* the b-plane; note that Bottke et al. 1996 have a slightly different, although essentially equivalent, definition), its coordinates x, y, z in the planetocentric rotating frame are given by

$$\begin{aligned} x &= \xi\cos\phi + (\eta\sin\theta + \zeta\cos\theta)\sin\phi \\ y &= \eta\cos\theta - \zeta\sin\theta \\ z &= -\xi\sin\phi + (\eta\sin\theta + \zeta\cos\theta)\cos\phi; \end{aligned}$$

in particular, the coordinates of a point belonging to the b-plane, where $b_\eta = 0$ by definition, are given by (Greenberg et al. 1988)

$$b_x = b_\xi\cos\phi + b_\zeta\cos\theta\sin\phi \tag{A8}$$
$$b_y = -b_\zeta\sin\theta \tag{A9}$$
$$b_z = -b_\xi\sin\phi + b_\zeta\cos\theta\cos\phi. \tag{A10}$$

These are then the steps to set up the Monte Carlo experiments described in the text in which encounters within b_{max} are computed using Öpik's theory:

1. a set of initial a, e, i is chosen from the given distribution;
2. a pair b_ξ and b_ζ is chosen at random between $-b_{max}$ and b_{max};
3. if $b = \sqrt{b^2_\xi + b^2_\zeta} < b_{max}$ the pair is retained;
4. x_{min}, x_{max}, z_{min}, z_{max} are determined from
$$\begin{aligned} x_{min} &= -\min(b_{max}, 1-q) \\ x_{max} &= \min(b_{max}, Q-1) \\ z_{min} &= -\min(b_{max}, \sin i) \\ z_{max} &= \min(b_{max}, \sin i); \end{aligned}$$
5. b_x and b_z are determined from (A8) and (A10);
6. if $x_{min} < b_x < x_{max}$ and $z_{min} < b_z < z_{max}$ the pair is retained;
7. the value of $\psi = \arcsin(b_\xi/b) = \arccos(-b_\zeta/b)$ is computed.

Appendix B: displacements in the energy vs. Tisserand parameter diagrams

Consider a comet with orbital elements a_0, e_0 and i_0; in Fig. 8 it is located at

$$x_0 = -\frac{a_p}{a_0} - 2\sqrt{\frac{a_0(1-e_0^2)}{a_p}}\cos i_0 \tag{B1}$$

$$y_0 = -\frac{a_p}{a_0} \tag{B2}$$

in the diagram relative to planet p.

If the comet is perturbed by a close encounter with planet p' into a new orbit with elements a, e and i, we want to compute the new coordinates x and y in the diagram relative to planet p. Obviously, the new coordinate y will be

$$y = -\frac{a_p}{a}; \tag{B3}$$

to compute x, we have to take into account the conservation of the Tisserand parameter relative to planet p', so that we have (note that the following considerations are valid only if the orbits of the two planets p and p' are circular and coplanar)

$$\frac{a_{p'}}{a} + \sqrt{\frac{a}{a_{p'}}}\Theta = \frac{a_{p'}}{a_0} + \sqrt{\frac{a_0}{a_{p'}}}\Theta_0; \tag{B4}$$

where we have put

$$\Theta = 2\sqrt{1-e^2}\cos i \tag{B5}$$

$$\Theta_0 = 2\sqrt{1-e_0^2}\cos i_0. \tag{B6}$$

We thus get

$$\Theta = \frac{\sqrt{a_{p'}^3}}{a_0\sqrt{a}} - \frac{\sqrt{a_{p'}^3}}{\sqrt{a^3}} + \frac{\sqrt{a_0}}{\sqrt{a}}\Theta_0, \tag{B7}$$

so that we can compute x

$$\begin{aligned} x &= -\frac{a_p}{a} - \sqrt{\frac{a}{a_p}}\Theta \\ &= -\frac{a_p}{a} - \frac{a_{p'}}{a_0} + \frac{a_{p'}}{a} - \frac{\sqrt{a_0}}{\sqrt{a_p}}\Theta_0 \\ &= y(1-\frac{a_{p'}}{a_p}) - \frac{a_{p'}\sqrt{a_p} + \sqrt{a_0^3}\Theta_0}{\sqrt{a_p}a_0}. \end{aligned} \tag{B8}$$

We therefore have that the close encounters with planet p' cause displacements, in the $-a_p/a$ vs. $-T_p$ diagram, along a straight line of slope $a_p/(a_p - a_{p'})$; since a particle with the same orbital parameters as planet p', i.e. $a = a_{p'}$, $e = i = 0$, would have with respect to this planet $T_{p'} = 3$, and would be located in the $-a_p/a$ vs. $-T_p$ diagram on the circular limit, it then follows that the straight line $T_{p'} = 3$ is tangent to the circular limit (for $i = 0$) at the location of planet p', and all the other straight lines $T_{p'}$ =const. are parallel to it.

References

Bailey M.E., Stagg C.R. 1990, Icarus, 86, 2

Bailey M.E., Chambers J.E., Hahn G. 1992, A&A, 257, 315

Belyaev N.A., Kresák Ľ., Pittich E.M., Pushkarev A.N. 1986, Catalogue of Short-Period Comets, Veda, Bratislava

Bottke W.F., Greenberg R., Carusi A., Valsecchi G.B. 1996, Mapping the effects of distant perturbations on particle-planet interactions, submitted to Icarus

Carusi A., Kresák Ľ., Valsecchi G.B. 1981, A&A, 99, 262

Carusi A., Kresák Ľ., Perozzi E., Valsecchi G.B. 1985, Long-Term Evolution of Short-Period Comets, Hilger, Bristol

Carusi A., Kresák Ľ., Perozzi E., Valsecchi G.B. 1987, A&A, 187, 899

Carusi A., Valsecchi G.B., Greenberg R. 1990, Celest. Mech., 49, 111

Carusi A., Kresák Ľ., Valsecchi G.B. 1995, Electronic Atlas of Dynamical Evolutions of Short-Period Comets, available in electronic form at URL http://titan.ias.fra.cnr.it/ias-home/comet/catalog.html

Duncan M., Quinn T., Tremaine S. 1988, ApJ, 328, L69

Everhart E. 1969, AJ, 74, 735

Everhart E. 1985, In Dynamics of Comets: their Origin and Evolution, eds. A. Carusi, G.B. Valsecchi, D. Reidel, Dordrecht, p. 185

Fernández J.A. 1980, MNRAS, 192, 481

Greenberg R., Carusi A., Valsecchi G.B. 1988, Icarus, 75, 1

Kresák Ľ. 1972, in The Motion, Evolution of Orbits, and Origin of Comets, eds. G.A. Chebotarev, E.I. Kazimirchak-Polonskaya, B.G. Marsden, D. Reidel, Dordrecht, p. 503

Kresák Ľ. 1982, in Sun and Planetary System, eds. W. Fricke, G. Teleki, D. Reidel, Dordrecht, p. 361

Kresák Ľ. 1994, in Asteroids, Comets, Meteors 1993, eds. A. Milani, M. Di Martino, A. Cellino, D. Reidel, Dordrecht, p. 77

Levison H.F., Duncan M.J. 1994, Icarus, 108, 18

Manara A., Valsecchi G.B. 1991, A&A, 249, 269

Marsden B.G., Williams G.V. 1992, Catalogue of Cometary Orbits, Central Bureau for Astronomical Telegrams, Cambridge

Nacozy P.E. 1976, AJ, 81, 787

Oikawa S., Everhart E. 1979, AJ, 84, 134

Öpik E.J. 1976, Interplanetary Encounters, Elsevier, New York

Quinn T., Tremaine S., Duncan M. 1990, ApJ, 355, 667

Tancredi G., Lindgren M., Rickman H. 1990, A&A, 239, 375

Valsecchi G.B. 1992a, In Periodic Comets, eds. J.A. Fernández, H. Rickman, Universidad de la República, Montevideo, p. 81

Valsecchi G.B. 1992b, In Periodic Comets (First round table: Dynamics of periodic comets), eds. J.A. Fernández, H. Rickman, Universidad de la República, Montevideo, pp. 98-100

This article was processed by the author using Springer-Verlag LaTeX A&A style file *L-AA* version 3.